3rd Micro and Nano Flows Conference
Thessaloniki, Greece, 22-24 August 2011
Keynote Contribution

On-Chip Micro-Evaporation: Experimental Evaluation of Liquid Pumping and Vapor Compression Cooling Systems

John R. THOME [1], Jackson B. MARCINICHEN [1,*]

* Corresponding author: Tel.: +41 21 693 5894; Fax: +41 21 693 5960; Email: jackson.marcinichen@epfl.ch
1: Laboratory of Heat and Mass Transfer (LTCM)
Faculty of Engineering (STI)
École Polytechnique Fédérale de Lausanne (EPFL)
Station 9, CH-1015 Lausanne, Switzerland

Abstract Thermal designers of data centers and server manufacturers are showing a great concern regarding the cooling of new generation data centers, which are more compact and dissipate more power than is currently possible to cool by conventional air conditioning systems. With very large data centers exceeding 100 000 servers, some consume more than 50 MW [1] of electrical energy to operate, energy which is directly converted to heat and then simply wasted as it is dissipated into the atmosphere. A potentially significantly better solution would be to make use of on-chip two-phase cooling [2], which, besides improving the cooling performance at the chip level, also adds the capability to reuse the waste heat in a convenient manner, since higher evaporating and condensing temperatures of the two-phase cooling system (from 60-95°C) are possible with such a new ***green*** cooling technology. In the present project, two such two-phase cooling cycles using micro-evaporation technology were experimentally evaluated with specific attention being paid to energy consumption, overall exergetic efficiency and controllability. The main difference between the two cooling cycles is the driver, where both a mini-compressor and a gear pump were considered. The former has the advantage due to its appeal of energy recovery since its exergy potential is higher and the waste heat is exported at a higher temperature for reuse.

Keywords: data center, microprocessor, on-chip two-phase cooling cycle, micro-evaporator, controller

1. Introduction

Under the current efficiency trends, the energy usage of data centers in the US is estimated to become more than 100 billion kWh by 2011, which represents an annual energy cost of approximately $7.4 billion [3]. With the introduction of a proposed carbon tax in the US [4], the annual costs could become as high as $8.8 billion by 2012, increasing annually. With the US having an annual increase of total electrical generation of approximately only 1.5% combined with the current growth rate of electrical energy by data centers being between 10-20% per annum (driven now even more by smart phones), data centers potentially will consume all of the electrical energy produced by 2050 if current growth rates continue! With air cooling of the servers in data centers accounting for most of the non-IT energy usage (up to 45% [5] of the total energy consumption), this is the logical energy consumer that needs to be attacked to reduce its wasteful use.

Nowadays, the most widely used cooling strategy is refrigerated air cooling of the data centers' numerous servers. When making use of this solution, nevertheless, 40% or more of the refrigerated air flow typically by-passes the racks of servers in data centers all together, according to articles presented at ASHRAE Winter Annual Meeting at Dallas (January, 2007), while also "cooling" thousands of servers that are not even in operation. This massive waste of energy motivates the search for a new green cooling solution to the future generation of higher performance servers that consume much less energy for their cooling. One promising solution is the application of on-chip two-phase cooling to dissipate the high heat flux densities of server CPU's. The most promising working fluids for these applications appear to be conventional refrigerants, for instance HFC134a, as opposed to low pressure dielectric coolants (such as FC-72) or water-cooling.

The goal of the present study was to evaluate the

performance of two different cooling cycles using micro-evaporator elements (multi-microchannel evaporators or ME's) for direct cooling of the chips and memories on a blade server board. The specific focus was to work with two-phase cooling using the dielectric refrigerant HFC134a, using a liquid pump (cycle 1) or a vapor compressor (cycle 2) to drive the working fluid, a micro-evaporator for cooling of the chip and for now a simple tube-in-tube condenser for heat recovery, which can reduce the demand of cooling energy by an impressive amount.

Experiments were done considering 2 ME's in parallel (typical for blade servers) whilst controlling the outlet vapor quality with an overdimensioned stepper motor valve (SMV), which modulates the mass flow with a neglegible pressure drop (called *cycle 1* here) or by speed control of a linear mini-compressor, permits direct modulation of the volumetric displacement (called *cycle 2* here). To represent the micro-processors, pseudo chips of 18 mm width and 12 mm length were installed in the test bench to be cooled by the ME's. Each pseudo chip was composed of 35 heaters (2.5 mm by 2.5 mm in size), which permits tests with non-uniform heat fluxes (hot spots). However, in the present work only uniform heat fluxes were considered. The refrigerant's condensing pressure (cycle 1) and the temperature difference in the counter-flow condenser (between outlet water flow and inlet refrigerant flow / cycle 2) were controlled by the condenser liquid pump speed (LPS), which modulates the mass flow rate of water in the condenser (secondary fluid). In summary, the main objectives were to evalute the flow distribution to the two parallel ME's and the average temperatures of the pseudo chips under transient conditions and different heat loads, primarily to investigate controllability and overall performance of these two cooling cycles. A preliminary exergy analysis was also performed, taking into account experiment results for the two-phase cooling system operating at steady state conditions. A brief literature review of other cooling systems and some basic fundamentals of multi-microchannel cooling is first presented before passing on to the current on-chip two-phase cooling system's design, tests and results.

2. Literature review

Hannemann *et al.* [6] proposed a pumped liquid multiphase cooling system (PLMC) to cool microprocessors and microcontrollers of high-end devices such as computers, telecommunications switches, high-energy laser arrays and high-power radars. According to them, their system could handle applications with 100 W heat loads (single chip) as well as applications with short time periods of 1000 W heat loads (radar). Their PLMC consisted of a liquid pump, a high performance cold plate (evaporator) and a condenser with a low acoustic noise air mover to dissipate the heat in the ambient air. A comparison between a single-phase liquid loop (water) and their two-phase system working with HFC134a was made for a 200 W heat load. Their HFC134a system had a mass flow rate, a pumping power and a condenser size that were 4.6, 10 and 2 times *smaller* than the water-cooled system they considered. The coolant temperature rise was 10 ˚C for the water but negligible for HFC134a. They emphasized the significant benefits of reduced pumping energy consumption, size and weight that were provided with the PLMC solution.

Mongia *et al.* [7] designed and built a small-scale refrigeration system applicable to a notebook computer. The system included a minicompressor, a microchannel condenser, a microchannel evaporator and a capillary tube as the throttling device and is considered to be the first refrigeration system developed that can fit within the tight confines of a notebook computer and operate with a high refrigeration efficiency. HC600a (isobutane) was the working fluid, chosen from an evaluation of 40 candidate refrigerants. According to them, HC600a presented the best efficiency at a low pressure ratio and was readily available. Although isobutane is flammable, the system required only a very small charge (a few milliliters). For a baseline operating condition, when the evaporator and condenser temperatures and the heat load were 50 ˚C, 90 ˚C and 50 W, respectively, the coefficient of performance (COP) obtained was 2.25. The COP reached 3.70 when the evaporator and condenser temperatures were increased and decreased by 10 ˚C from the baseline conditions and the heat load was reduced to 44 W. Their small-scale refrigeration system achieved 25-30% of Carnot efficiency (ideal COP for a Carnot cycle), values comparable with those obtained in today's household refrigerators.

Trutassanawin *et al.* [8] designed, built and evaluated

the performance of a miniature-scale refrigeration system (MSRS) suitable for electronics cooling applications. Their MSRS had the following components: a commercial small-scale compressor, a microchannel condenser, a manual needle valve as the expansion device, a cold plate microchannel evaporator, a heat spreader and two compressor cooling fans. A suction accumulator to avoid liquid flow to the compressor, an oil filter to return oil to the compressor and guarantee good lubrication, and heat sources to simulate the chips were also installed. HFC134a was the working fluid. System performance measurements were conducted at evaporator temperatures from 10 ˚C to 20 ˚C and condenser temperatures from 40˚C to 60˚C. The cooling capacity of the system was varied from 121 W to 268 W with a COP of 1.9 to 3.2 at pressure ratios of 1.9 to 3.2. Their MSRS was able to dissipate CPU heat fluxes of approximately 40-75 W/cm^2 while keeping the junction temperature below 85 ˚C for a chip size of 1.9 cm^2. It was concluded that a new compressor design for electronics cooling applications was needed to achieve better performance of the system (the most significant losses occurred in the compressor, which was not designed for the operating conditions of electronics cooling). They also recommended studying the development of an automatic expansion device and a suitable control strategy for the MSRS.

Thome *et al.* [9] surveyed the advances in thermal modeling for flow boiling of low pressure refrigerants in multi-microchannel evaporators for the on-chip two-phase cooling of microprocessors. According to that study, multi-microchannel evaporators hold promise to replace the actual air cooling systems currently in use and can compete well against water cooling to remove high heat fluxes, higher than 300 W/cm^2, while maintaining the chip safely below its maximum working temperature, while also providing a nearly uniform chip base temperature [10] and minimizing energy consumption. Variables such as critical heat fluxes, flow boiling heat transfer coefficients and two-phase pressure drops were evaluated and characterized as they are important design parameters of micro-evaporators used for high heat flux cooling applications.

Thome and Bruch [11] simulated two-phase cooling elements for microprocessors with micro-evaporation using a new inhouse simulation code developed specifically for that purpose. Heat fluxes of 50 W/cm^2 and 150 W/cm^2 in a micro-evaporator with channels 75 μm wide, 680 μm high and 6 mm long with 100 μm thick fins were simulated for flow boiling. The size of the chip was assumed to be 12 mm by 18 mm and the micro-evaporator was considered with the fluid inlet at the centerline of the chip and outlets at both sides, i.e. a split flow design to reduce the pressure drop but increase the critical heat flux. Simulation results of pumping power, critical heat flux, and junction and fluid temperatures were generated using the best thermal design methods available in the literature, considering operation with HFC134a at an inlet saturation temperature of 55 ˚C (chosen to allow for heat recovery). The following conclusions were reached: (i) the influence of mass flux on the fluid, chip and wall temperatures was small, (ii) for the heat flux of 150 W/cm^2, the chip temperature was 70 ˚C or less, well below its operational limit of 85 ˚C, (iii) the junction-to-fluid temperature difference was only 15 K for the heat flux of 150 W/cm^2, which is lower than that with water cooling systems, (iv) there was a margin for the fluid working temperature to be raised by 10 K to a junction temperature of 80 ˚C while rejecting heat at 65 ˚C for reuse, and (v) the critical heat flux increased with the mass flux and the lower limit was about 150 W/cm^2 for 250 kg/m^{2}s. The channel width had a significant effect on the wall and junction temperatures, and there was a turning point at about 100 μm when considering 1000 kg/m^{2}s of mass flux and 150 W/cm^2 of base heat flux, at which these temperatures reached a minimum. For the same mass flux and base heat flux, the reduction of channel width also reduced the energy consumption to drive the flow (pumping power).

From a microcooling element viewpoint, Thome and Bruch [11] showed an approximate comparison of performances of liquid water cooling versus two-phase cooling. For the same pumping power consumption to drive the fluids through the cooling element on the CPU, two-phase cooling allowed the chip to operate about 13 K cooler than water cooling or it could operate at the same junction temperature but consume much less pumping power using a lower refrigerant flow rate. Thus, based on their simulations, a two-phase cooling system appeared to be more energy-efficient than classical air cooling or water cooling systems while also exhausting the heat at higher reusable temperatures. Regarding the choice between a pump or a compressor as the driver for a micro-evaporation heat sink system, they emphasized

that the choice depends on the economic value of the re-used energy. The system with a compressor is ideal for energy re-use because of the higher heat rejection temperature; however the additional energy consumed by the compressor compared to the pump has to be justified by the re-use application (but that additional energy is also recoverable as waste heat).

Mauro *et al.* [12] evaluated the performance of a multi-microchannel copper heat sink with respect to critical heat flux (CHF) and two-phase pressure drop. A heat sink with 29 parallel channels (199 μm wide and 756 μm deep) was tested experimentally with a split flow system with one central inlet at the middle of the channels and two outlets at either end. Three working fluids were tested (HFC134a, HFC236fa and HFC245fa) and also the parametric effects of mass velocity, saturation temperature and inlet temperature. The analysis of their results showed that a significantly higher CHF was obtainable with the split flow system compared to the single inlet-single outlet system [13], providing also a much lower pressure drop. For the same mass velocity, the increase in CHF exceeded 80% for all working fluids evaluated, due to the shorter heated length of a split system design. For the same total refrigerant mass flow rate, an increase of 24% for HFC134a and 43% for HFC236fa were obtained (no comparable data were available for HFC245fa). They concluded that the split flow system had the benefit of much larger CHF values with reduced pressure drops and further developments in the design of split flow system could yield an interesting energetic solution for cooling of computer chips.

Zhou *et al.* [14] developed a steady-state model of a refrigeration system for high heat flux electronics cooling. The refrigeration system proposed consisted of multiple evaporators (microchannel technology), a liquid accumulator with an integrated heater, a variable speed compressor, a condenser and electric expansion valves (EEV). To obtain more efficient heat transfer and higher critical heat flux, the evaporators were considered to operate only with two-phase flow. To guarantee the safe operation of the refrigeration system, these authors considered the presence of an integrated heater-accumulator to fully evaporate the two-phase flow coming out of the evaporator, which naturally represents a decrease of the cycle COP. A parametric study to evaluate the effects of external inputs on the system performance (secondary fluid temperature in the condenser, evaporator heat load, compressor speed, EEV percentage opening and heat supplied to the accumulator) and a Pareto optimization to find the optimal system operating conditions were also developed. Heat loads of 1500 W and 2500 W, which represent heat fluxes of 9.4 W/cm^2 and 15.66 W/cm^2, were considered. Their main conclusions were: (i) the system COP could be improved without compromising the critical heat flux when handling higher heat fluxes, (ii) higher critical heat fluxes are achievable with a smaller EEV opening and higher heat input supplied to the accumulator and (iii) a trade-off between the system COP and CHF is necessary to prevent device burnout, i.e. the imposed heat flux must be lower than the critical heat flux including a safety margin. Finally, they presented a preliminary validation of the model with initial experimental data showing a satisfactory prediction ability of the model. The authors do not mention anything about the geometry assumed for the evaporators.

Zhang *et al.* [15] evaluated the effect of transient heat loads on inherent pressure drop flow instabilities in two-phase refrigeration cooling systems. These authors identified such instabilities with the negative slope of the boiling flow pressure drop with the increase of mass flux. The idea would be to develop a controller capable of compensating the portion of the boiling flow pressure drop curve with a negative slope, so that no flow excursion or oscillation would take place, i.e. the combined system pressure drop increases monotonically with mass flux. A two-loop refrigeration system was assumed for two-phase cooling of ultra high power electronic components for their simulations where the primary loop was composed of a pump, a surge tank, an accumulator and cartridge heaters imersed in the refrigerant (HFC134a) to emulate the evaporator. Their second loop consisted of a vapor compression cycle, which dissipated the waste heat to the ambient by using a fluid-to-fluid heat exchanger. A set of active control strategies were developed to suppress compressible flow boiling oscillations and to maintain reasonable electronic wall temperatures under transient heat load changes. Simplified two-phase friction and heat transfer correlations were used to design and simulate the controllers, since no widely-accepted transient two-phase heat transfer model was found in the literature. Periodic heat load changes for periods varying from 2 s, 5 s, and 10 s within the simulation

time range (10 – 50 s) for a heat load variation amplitude of 500 W were simulated. Two actuators were evaluated, a valve before the heated channel and a supply pump. According to the authors, although the valve could suppress the compressible flow instability, it suffers from high pressure loss and high pumping power consumption. The use of a positive displacement pump could also regulate the downstream flow and the valve could be removed so that no additional pressure loss is induced. In summary, the results of their simulations showed that both actuators were efficient and effective to control the flow oscillations. However, no experimental evaluations of these systems were done to confirm their conclusions.

Marcinichen *et al.* [16] simulated a vapor compression cycle and a pumped cooling cycle using on-chip cooling with multi-microchannel evaporators. According to the authors the vapor compression cycle is characterized by a high condensing temperature (high heat recovery potential, i.e. high exergy) and a high range of controllability of the micro-evaporator inlet subcooling (characteristic of systems with variable speed compressor and electric expansion valve), but it has a high energy consumption. The pump's cycle instead is characterized as having a low condensing temperature (similar to the evaporating temperature in the micro-evaporator), and its energy consumption is low. Marcinichen *et al.* [17] developed a simulation code to evaluate such cycles. A total of 5 cases were simulated considering 3 different working fluids, HFC134a, HFO1234ze and single-phase water (in an analogous single-phase cooling cycle) with different internal diameters of the pipes and elbows joining the components. HFO1234ze is a new environmentally-friendly refrigerant of Honeywell Inc. expected to replace HFC134a in such systems. The results showed that for a design of the cooling cycle such that the total system pressure drop was about 1.5 bar (not just that attributable to the micro-cooler on the CPU as in most previous studies), the liquid water cooling cycle had a pumping power consumption 5.5 times that obtained for the two-phase HFC134a cooling cycle, both considering a liquid pump as the driver of the fluid. When compared with the HFO1234ze cooling cycle, which showed a total pressure drop of 1.79 bar, the difference drops to 4.4 times. These results can be considered the cooling system differential when compared with demonstration projects (excluding the energy consumption of the secondary fluid that removes the heat away from the rack), such as that for the new high performance computer called AQUASAR [18, 19, 20], which actually implemented a liquid water cooling cycle on an IBM rack cabinet with a power consumption of around 10 kW. The simulation of a vapor compressor cooling cycle showed higher pumping power consumption when compared with the other cycles simulated; however, this cycle can be justified when the waste heat at the condenser is recovered for applications such as district heating and preheating of boiler feedwater. The highest condensing temperature (higher secondary fluid temperature) and heat transfer rate (associated with the work imparted by the compressor) represents a higher economic value than that obtained with the liquid pump cooling cycles. The present study is a continuation of the two simulation studies above. The two two-phase cooling cycles were built into one multi-purpose test bench facility and experimentally evaluated under various typical blade server operating conditions of transient, steady state, balanced and unbalance heat loads on the system's two pseudo CPU's. Aspects such as controllability, energy consumption and exergy avaliable in the condenser were investigated.

3. Multi-microchannel elements

General fundamentals

Before describing the test set up and its results, a brief overview of microchannel heat transfer is first given, as this in the most important element of the cooling system. While initial studies in the literature reported significant size effects on friction factors and heat transfer coefficients in very small channels in single-phase flows, more accurate tests and analysis done with very smooth internal channels have shown that macroscale methods for single-phase flows work well at least down to diameters of 5-10 μm [21]. This is *not* the case for macroscale two-phase flow methods, which usually do not work very well when compared to data for channels below about 2.0 mm diameter. Thus, it is inappropriate (unreliable) to extrapolate macroscale research results and methods to the microscale. Furthermore, many of the controlling phenomena and heat transfer mechanisms change when passing from macroscale two-phase flow and heat transfer to the microscale. For example, surface tension (capillary) forces become much stronger as the

channel size diminishes while gravitational forces are weakened. Or, for example, many two-phase microchannel flows have *laminar* liquid Reynolds numbers whereas most macroscale methods are based on *turbulent* two-phase flow data. Furthermore, the nucleate boiling contribution of macroscale flow boiling is more or less suppressed in microchannels. Therefore, dedicated research is required to investigate these microscale two-phase flows and develop new models and methods to describe them.

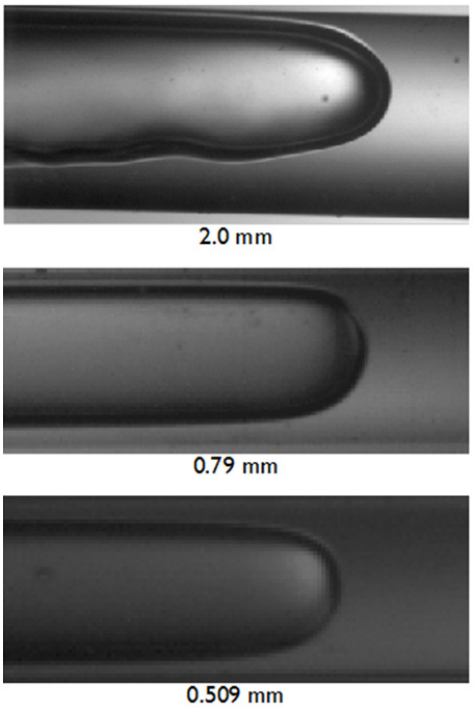

Figure 1 Video images of slug (elongated bubble) flow in 2.0, 0.8 and 0.5 mm horizontal channels with HFC134a.

As a first view, Figure 1 depicts the buoyancy effect on elongated bubbles flowing in 2.0, 0.790 and 0.509 mm horizontal circular channels taken in the LTCM lab [22]. In the 2.0 mm channel, the difference in liquid film thickness at the top compared to that at the bottom of the bubble is very noticeable. Since the local heat transfer is primarily by conduction across such thin laminar liquid films, the film thickness is the main resistance to heat transfer and thus cooling, and therefore its variation around the perimeter is an important thermal issue. Similarly, the film thickness in the 0.790 mm channel is still not uniform above and below the bubble. Instead, in the 0.509 mm channel, the film is now quite uniform. Interpreting these images and other images, one also ascertains that in small, horizontal channels that stratified types of flows (all vapor at top with liquid at the bottom) disappear. This transition is thus perhaps an indication of the lower boundary of macroscale two-phase flow, in this case occurring for a diameter somewhat greater than 2.0 mm. The upper boundary of microscale two-phase flow may be interpreted as the point at which the effect of gravity on the liquid-vapor interface shape becomes insignificant, such that the uniformly flowing bubble in the 0.509 mm channel is thus a microscale flow, with the transition occurring at about this diameter at the present test conditions.

Heat transfer and pressure drop mechanisms are strongly affected by the type of flow patterns present in the channels, which need to be determined to develop prediction methods. With the aid of high-speed videography (videos up to 120'000 digital images per second) and laser photo diode signals, it is possible to record and characterize these regimes. Figure 2 shows a typical flow pattern map for HFC236fa inside a channel having a diameter of 1.03 mm obtained by Revellin *et al.* [22]. The flow patterns are classified as isolated bubbles (mostly bubbles shorter in length than the channel diameter), coalescing bubbles (mostly bubbles much longer than the channel diameter and coalescing due to their different axial velocities) and annular flow (characterized by a thin liquid film on the channel perimeter with a high speed vapor core flow).

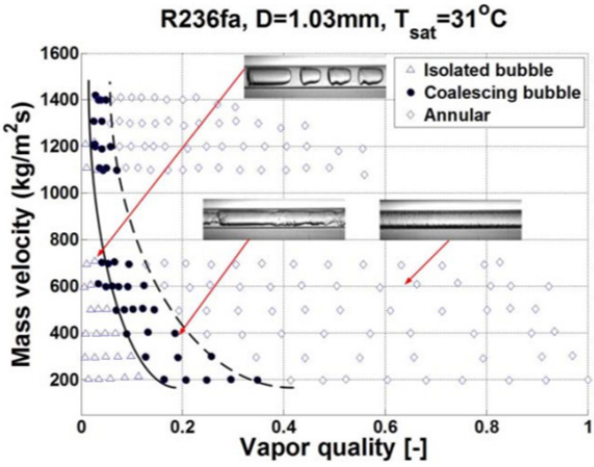

Figure 2 Three flow regimes shown on a flow pattern map [23].

Micro-evaporators

It was proven experimentally that, using a refrigerant

evaporating at 60 ˚C, microprocessors could be kept well below their 85 ˚C limit, while removing heat fluxes in excess of 180 W/cm^2 or more [24]. Two-phase flow is also ideally suited for cooling of electronic hot-spots (local heat fluxes on CPU's up to 400 W/cm^2 or more) as heat transfer coefficients (thermal resistances) naturally increase (decrease) over hot-spot locations in the flow boiling process, according to numerous uniform heat flux test data. This has the implication that electronics can have a more uniform temperature with two-phase cooling, implying that problems associated with adverse temperatures gradients are greatly diminished and hence higher clock speeds can potentially be utilized. The power requirements for removing the heat are also considerably lower than required for traditional air-cooling methods. This is due to the much larger heat carrying capacity of evaporating refrigerants than air.

Numerous other aspects of these microscale two-phase flows are under investigation in the LTCM lab, such as micro-PIV to characterize flow (with or without flashing) through micro-orifices as small as 15-25 microns, transient aspects of the two-phase flow bubble coalescence process [25], time-strip analysis of high speed videos to discern information on the dry out process and wave formation [26], flow pattern transition theory [23], two-phase hot-spot cooling [27], critical heat flux [28], etc. All these aspects are focused solely on the micro-evaporator. To see the actual effect on the cooling performance of a data center, such on-chip micro-evaporators need to be analyzed as part of a complete cooling cycle to determine their actual energetic characteristics.

A detailed discussion, including thermal design methods, on two-phase flow and heat transfer in microscale channels can be found in the free web-book Wolverine Engineering Databook III of Thome [29].

4. Hybrid cooling cycle

Figure 3 and Figure 4 depict potential two-phase cooling cycles, in which the cycle drivers are a liquid pump and a vapor compressor, respectively [16]. The goal is to control the chip temperature to a pre-established level by controlling the inlet conditions of the multi-microchannel cooler (pressure, subcooling and mass flow rate). It is imperative to keep the multi-microchannel cooler outlet vapor quality below that of the critical vapor quality, which is associated with the critical heat flux. Due to this exit vapor quality limitation (it is suggested not to surpass one-half of the critical vapor quality at the evaporator exit as a tentative safety margin), additional latent heat is available for further two-phase cooling in the server, which can be safely done for other low heat flux generating components, such as memory, DC/DC converters, etc.

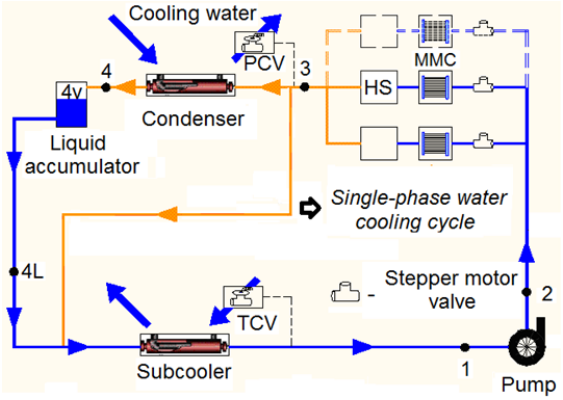

Figure 3 Schematic of the liquid pumping cooling cycle.

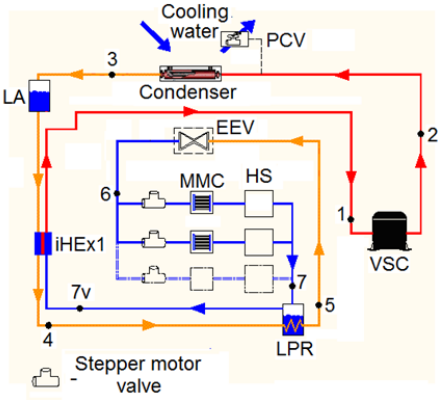

Figure 4 Schematic of the vapor compression cooling cycle.

Another parameter that must be controlled is the condensing pressure (condensing temperature). The aim is to recover the energy dissipated by the refrigerant in the condenser to heat buildings, residences, district heating, pre-heating boiler feedwater, etc. when it can be arranged and is viable.

The liquid pumped two-phase cooling cycle can be characterized by its having low initial costs, a low vapor quality at the on-chip multi-microchannel cooler

(MMC) outlet, a high overall efficiency, low maintenance costs and a low condensing temperature. The heat spreader (HS) is for cooling of memory, etc., which is shown as "one" cooler here for simplicity purposes. This is a good operating option when the energy dissipated in the condenser is not recovered, typically during the summer season. However, the heat can still be recovered if there is an appropriate demand for low quality heat (low exergy) at about 60 °C. On the other hand, the vapor compression cooling cycle can be characterized as having a high condensing temperature of up to 90-100°C (high heat recovery potential), a high range of controllability of the MMC inlet subcooling (characteristic of systems with variable speed compressors, VSC's, and electric expansion valves, EEV's), and a medium overall efficiency when compared with the liquid pumping cooling cycle. This is a good operating option when the energy dissipated in the condenser is recovered for other uses, typically during the winter season when considering a district heating application (high exergy).

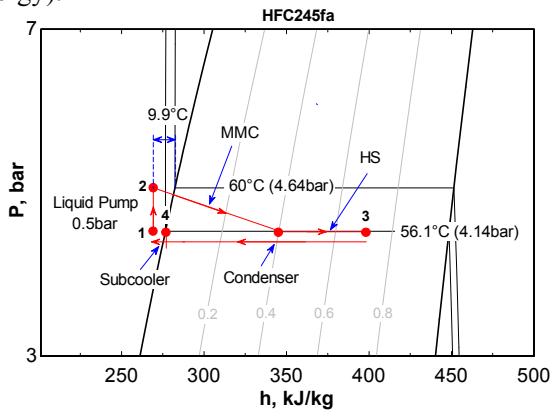

Figure 5 P-h diagram of the liquid pumping cooling cycle.

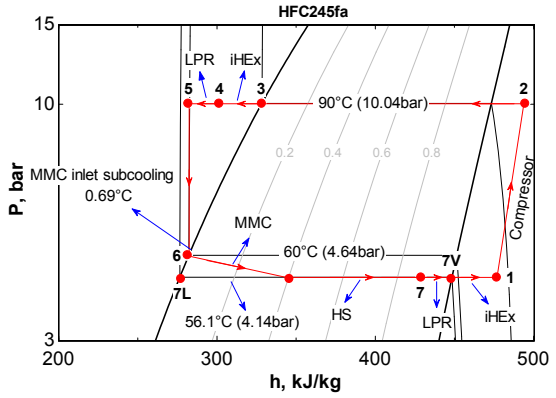

Figure 6 P-h diagram of the vapor compression cooling cycle.

Figure 5 and Figure 6 show the Mollier diagrams of the two cooling cycles for HFC245fa as the working fluid [16]. It can be noticed that the two cycles are differentiated mainly by the condensing temperatures with the evaporating temperature of the MMC set at 60 °C (sufficient to keep the CPU below 85 °C).

It is worth mentioning that the applicability of these cooling cycles is not restricted to only one microprocessor but can be applied to blade servers and clusters, which may have up to 70 blades per rack. Each blade, such as that of IBM shown in Figure 7, can have two or more microprocessors with a heat generation capacity of about 90 W each. If the auxiliary electronics (memories, DC/DC, etc.) on the blade are included, the total heat generation per blade can be 350 W or more. Thus, the heat spreader (HS), shown earlier in Figure 3 and Figure 4, has the function to cool the auxiliary electronics, which can represent about 50% of the total heat load on the blade, but will have a larger surface area compared to the CPU and thus a lower heat flux.

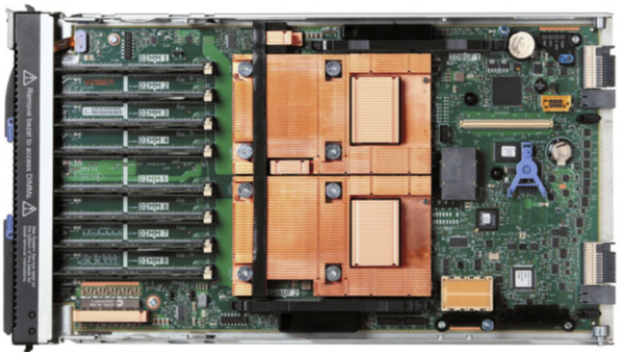

Figure 7 IBM blade with two microprocessors and heat generation capacity of 350 W [30].

Consequently, when considering an entire rack, a very sizable heat load is generated, representing a good opportunity to recover the heat rejected. In this case, reuse of the heat removed from the blades for a secondary application will greatly reduce the CO_2 footprint of the system. For example, if we consider a data center with 50 racks packed with high density blade servers (70 per rack), with each blade dissipating 350 W, the total potential heat to be recovered is 1.225 MW. Such a heat recovery system requires a secondary heat transfer fluid to pass through all the condensers (either water or a refrigerant) to transport the heat to its destination (to the environment or into a heat recovery system).

5. Experiments

The liquid pumping and vapor compression cooling cycles showed previously were built and experimentally evaluated in the present study, investigating the cooling system's energy consumption, exergetic efficiency and controllability. For such an evaluation specific controllers were first designed and tested. The variables to be controlled were the MEs outlet vapor quality, the condensing pressure (LP cycle) and the temperature difference between the water outlet flow and working fluid inlet flow in the condenser (VC cycle). The actuators used were the vapor compressor, the condenser liquid pump and the stepper motor valve. Two MEs in parallel assembled on pseudo chips, each composed of 35 heaters and temperature sensors, were used. The ME's copper microchannel geometry was made with 1.7 mm and 0.17 mm channel height and width and 0.17 mm fin width. The effective "footprint" area of the MEs is 12 mm length and 18 mm width. HFC134a was tested as the working fluid and an oil free mini-compressor (supplied by Embraco) and a gear pump as drivers. It is important to highlight the characteristic "oil free", which is mandatory for operation of micro-evaporation cooling systems and is considered as an advantage of such minicompressor.

5.1. Liquid pumped cooling system

A. Controllers

The first controller developed was to modulate the condenser liquid pump speed (LPS) in order to maintain the condensing pressure (Pc) at the set point value (Pc_{sp}). The second controller was developed to control the MEs outlet vapor quality (x_o), but with the modulation of the stepper-motor-valve aperture (A_{SMV}). This was achieved by deriving mathematical models capable of representing the dynamic behavior of the system under consideration by means of a system identification process and a PI structure that was used for the controllers since the system showed low order dynamics.

What follows is the system identification, controller design and preliminary evaluation by tracking tests, which are conventional steps in the development of new controllers. In sequence, a deeper evaluation of the controllers operating together is shown for what was named dualSISO control strategy, which does not consider the coupling effects between the controlled variables. Such a strategy was evaluated by disturbance rejection and flow distribution tests, for the latter the effect of different heat loads applied on the two micro-evaporators is investigated.

- LPS controller: system identification and controller design

Figure 8 ilustrates the block diagram of the first control loop, where the condensing pressure (Pc) is the controlled variable (Pc_{sp} is the set point) and the condenser liquid pump speed (LPS) is the manipulated variable.

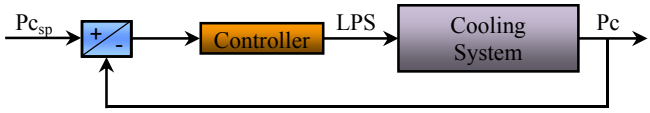

Figure 8 LPS controller

The system identification process has the objective of deriving a mathematical model capable of representing the dynamic behavior of the system. A linear first-order model with delay was used to correlate Pc with the LPS variations. The condensing pressure was measured with a calibrated pressure transducer at the inlet of the condenser. For such a system, the pressure drop between the inlet of MEs and inlet of condenser is neglegible, so the condensing pressure controller can also be considered as an evaporating pressure controller. Equations 1 and 2 show the model in the time and Laplace domains, respectively:

$$\tau \frac{dy(t)}{dt} + y(t) = K_P u(t - \theta) \quad (1)$$

$$G(s) = \frac{y(s)}{u(s)} = \frac{K_P e^{-\theta s}}{\tau s + 1} \quad (2)$$

The input (u) and output (y) parameters are LPS and Pc, respectively while G is the transfer function, τ the system time constant, K_P the gain and θ the transport delay.

The model parameters were obtained by varying the LPS from 1620 rpm to 1800 rpm (step response experiment, *viz.* Figure 9). The cycle's liquid pump speed, the water temperature (secondary fluid) at the inlet of condenser, the SMV's aperture and the heat

load on the MEs were maintained at 3000 rpm, 40 °C, 25%, and 90 W for ME1 and 75 W for ME2, respectively. These operating conditions are from now on referred to as the *standard conditions*.

It is important to mention that during the initial tests it was observed that the subcooler was redundent for this cycle and level of heat load investigated. This was due to the heat losses in the piping, which ensured that there was enough subcooling at the inlet of the liquid pump and micro-evaporators. Such a situation might not be the same for the case of better piping insulation and higher heat load, as for an entire blade center (e.g. IBM blade center QS22 with a heat load of about 5000 W). The subcooling at the inlet manifold of the MEs in all evaluations considered in this work remained between 2 °C and 8 °C, avoiding the necessity for special controllers to avoid saturation conditions (that is, unwanted vapor in the inlet header of ME1 and ME2), which would otherwise jeopardize the MEs performance by creation of flow maldistribution.

The model parameters K_P, τ and θ were estimated in order to minimize the square error between the model predictions and the experimental data. For this controller K_P, τ and θ were estimated as -0.8 mbar/rpm, 90.85 s and 2.59 s, respectively. Figures 9 and 10 depict part of the identification tests, showing the Pc response to a step change in the LPS and also the Pc model predictions against the experimental data.

As mentioned beforehand, the PI structure was selected for this study. Equation 3 shows the PI controller transfer function in the Laplace domain.

$$C(s) = K_C\left(1 + \frac{1}{T_I s}\right) \tag{3}$$

The PI controller was designed using the method proposed by [31], which is based on linear programming. It was computed to guarantee a phase margin of 30°, a gain margin of 2 and a crossover frequency two times larger than in an open loop. The T_I (integral time) and K_C (proportional) parameters were calculated as 90.85 s and -9816 bar/rpm, respectively.

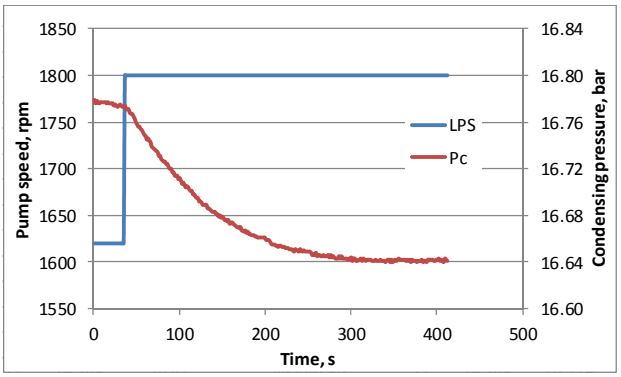

Figure 9 LPS - model identification

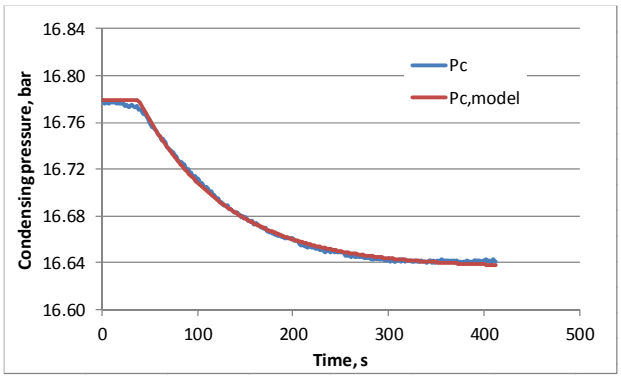

Figure 10 LPS - experimental vs. prediction

- Controller evaluation

Tracking tests were carried out with the experimental apparatus running under the *standard operating conditions* to evaluate the controller performance. Figures 11 and 12 show the results for five steps in the pressure set point between 16.8 bar and 17.0 bar for the LPS controller. As can be noticed, the controller increased or decreased the liquid pump speed, in response to a decrease or increase in the pressure set point value.

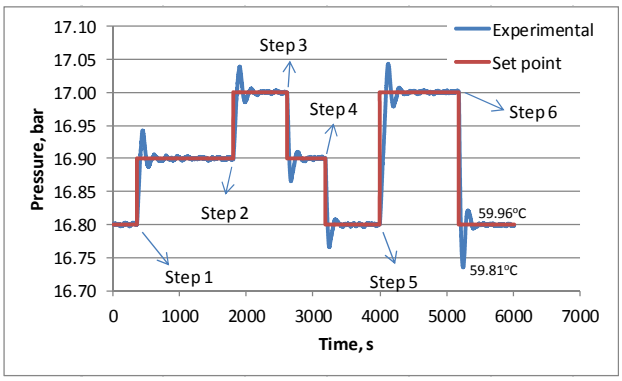

Figure 11 Pc variation

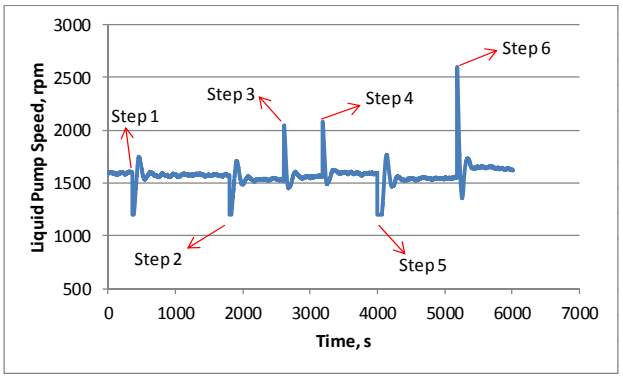

Figure 12 LPS variation

The results showed that the controller is effective and efficient to track the set point of pressure in a short time (≅ 3.5 min after step 6, *viz.* Figure 13) with a maximum overshoot in the condensing temperature of only about 0.16 °C (*viz.* Figure 11).

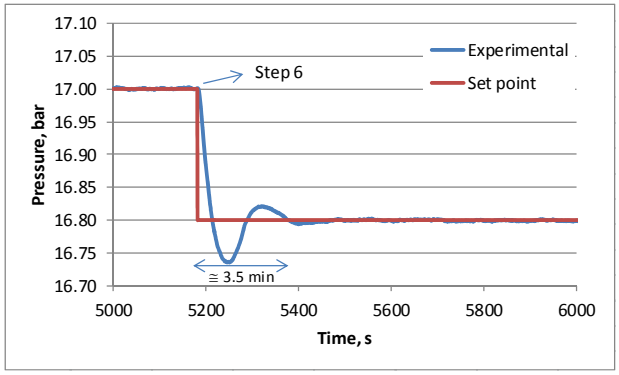

Figure 13 Pc variation for step 6

- SMV controller: system identification and controller's design and evaluation

The controller developed for the MEs' outlet vapor quality considered the SMV as the actuator. The vapor quality of the flow after the outlet of the MEs was used for control. It is worth mentioning that this variable has a considerable effect on the performance of the ME [32], and as a consequence on the overall system. Therefore, for safe operating reasons, such a controller must avoid the critical vapor quality, a condition where the pseudo chips could be damaged due to dryout occuring. Figure 14 illustrates the controller's block diagram.

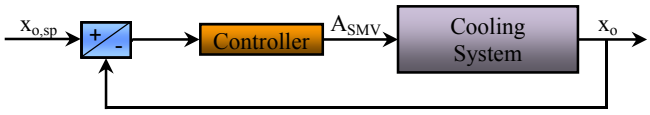

Figure 14 SMV controller

The system identification was developed considering the *standard conditions* as a starting point and a change in SMV aperture of 2% each 10s between 22% and 50% of aperture. The average of vapor quality for the last 5 seconds of each change was considered as the value for each aperture, i.e. the values shown in the Figure 15. It is important mentioning that the vapor quality was calculated/determined for each acquisition time by an energy balance enclosing the MEs, where the variables heat load, mass flow rate and inlet/outlet pressures and temperatures, required for this calculation, were measured with calibrated transducers.

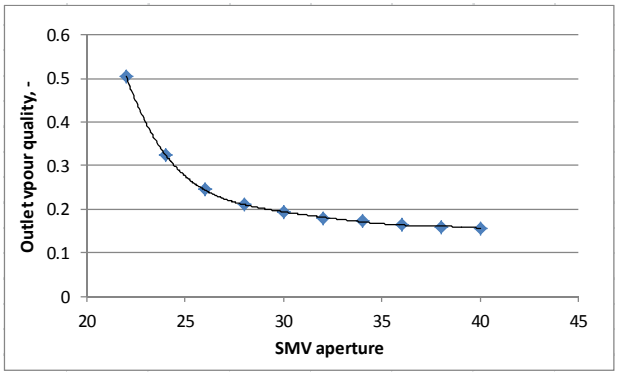

Figure 15 System identification: x_o vs. SMV aperture

During the system identification it was observed that small changes in the aperture resulted in a fast response (2s…3s) in the exit vapor quality, as can be seen in Figure 16. Thus, the model of the system was approximated by its static gain (K_p), which varied nonlinearly with the SMV aperture change, as can be seen in Equation 4.

$$K_P = \frac{\partial X}{\partial SMV} = -7.8.10^{-6} SMV^4 + 10.4.10^{-4}.SMV^3 - 5.2.10^{-2} SMV^2 + 1.16 SMV - 9.63 \quad (4)$$

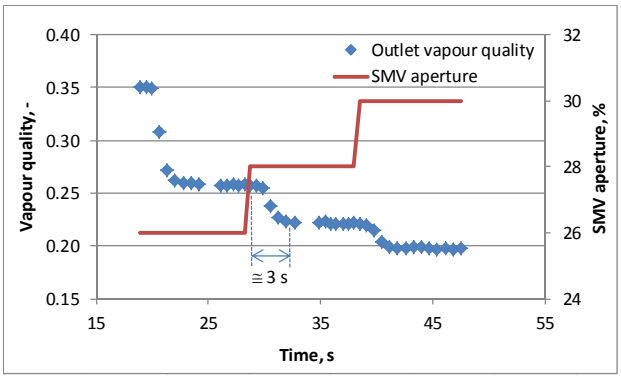

Figure 16 System identification: response time of exit vapor quality by changing the SMV aperture.

Therefore, a gain-scheduled PI controller was developed whose gain was a function of the SMV aperture. That is, the closed loop transfer function was represented by Equation 5, where the time constant (τ) is given by Equation 6:

$$H(s)=\frac{x_o}{x_{o,sp}}=\frac{\frac{K_c}{K_i}s+1 \quad \{zeros}{\frac{s(1+K_c.K_p)}{K_i.K_p}+1 \quad \{poles} \tag{5}$$

$$\tau=\frac{1+K_c.K_p}{K_i.K_p} \tag{6}$$

Defining τ_D as the desired closed loop time constant, and C as a parameter relating the closed loop pole (p) and zero (z) such that $p = C.z$, Equations 7 and 8 were obtained for the integral and proportional constants, i.e. K_I and K_C:

$$K_C=\frac{1}{(C-1).K_P} \tag{7}$$

$$K_I=\frac{C}{C-1}.\frac{1}{\tau_D.K_P}=\frac{T_I}{K_C} \tag{8}$$

The gains K_I and K_C of the controller are functions of the static gain of the system K_p and are updated during runtime. C and τ_D can be seen as tuning parameters, which were experimentally adjusted for 15 and 5 s, respectively. Moreover, an anti-wind up strategy was implemented to reduce the accumulated integral error of the controller when the output of the control moved outside the SMV's range (22% to 50% of aperture). It is worth highlighting that other techniques to design the gain-scheduled controller could also be used, for example, the method proposed in [33].

Figure 17 shows the outlet vapor quality tracking test, where it can be seen that the controller reacted fairly quickly for the 4 steps considered. In the worst case, the controller took about 30 s to stabilize the system; however only a small overshoot was observed, i.e. maximum of 1.5% in vapor quality. Finally, it can be concluded that the controller was efficient and effective for the actual application, showing a small overshoot and settling time.

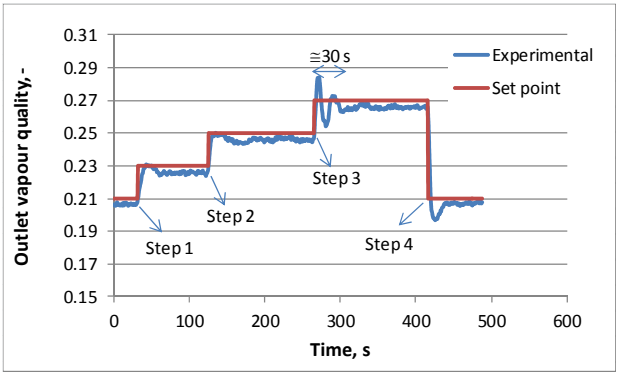

Figure 17 Outlet vapour quality tracking test.

B. Dual SISO controller

The dual SISO control strategy was derived from the two individual controllers, as illustrated in the block diagram of Figure 18. This allowed the simultaneous control of Pc and x_o to match the thermal load with the cooling capacity for the condensing temperature and vapor quality desired.

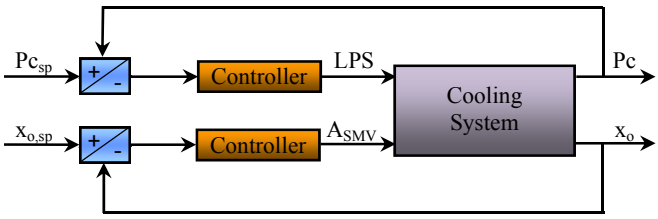

Figure 18 The dual SISO controller

Disturbance rejection and flow distribution tests were performed with the experimental apparatus running under a *standard operating condition* to evaluate the controllers' performance. In these tests, after the apparatus was in a steady-state regime, the input power on the pseudo chips (heat load on the MEs) was changed periodically for a constant period of time

between two levels for the disturbance rejection tests and changed to different levels until the steady state condition was established for the flow distribution tests, as can be seen below.

- Heat load disturbance rejection

The integrated controller or descentralized control structure was first evaluated by considering the *standard conditions* at the beginning of the test, and a set point of condensing pressure (Pc_{sp}) and outlet vapor quality of 16.8 bar and 22%, respectively. The performance of the control strategies regarding disturbance rejections were evaluated by periodically changing the heat load on the micro-evaporators. As the heat load changed, so did the condensing pressure and vapor quality disturbances, which were detected automatically by the controllers. These in turn increased or decreased the LPS and A_{SMV} to maintain the pressure and vapor quality at the set point.

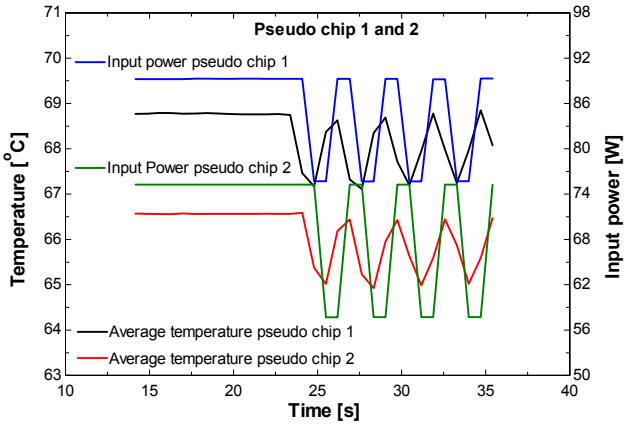

Figure 19 Heat load disturbance and pseudo chip temperatures

The heat load on ME1 and ME2 were changed between 90 W and 75 W and 75 W and 60 W, respectively, considering a periodic disturbance time of 1.4 s. Figure 19 shows the input power disturbance on the pseudo chips and the effect on the average temperature of each chip. This temperature was obtained by averaging the temperature from 11 well distributed sensors on each chip. It can be observed that there was a maximum temperature variation of 1.5 °C, which can be considered to be insignificant when compared to the temperature gradient along the chip for on-chip single-phase cooling using water (about 2 °C [18, 19, 20]).

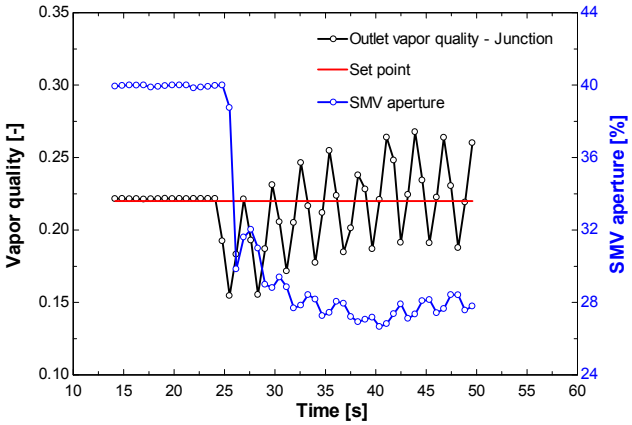

Figure 20 Outlet vapour quality and SMV controller

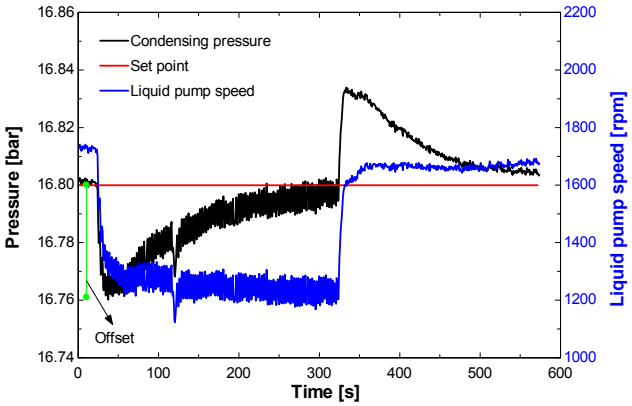

Figure 21 Condensing pressure and LPS controller

Figures 20 and 21 show the controllers' action under the situation of a disturbance. It can be seen that the SMV controller was able to maintain the exit vapor quality between a range of ±4% of the set point. What is important to observe is that the controller was effective, that is, it showed fast response for the induced disturbance and no instability was observed. The LPS controller (*viz.* Figure 21) showed an initial offset when the heat load disturbance started, which represents a condensing temperature deviation of only 0.05 bar or 0.1°C (it also represents a very small evaporating temperature variation) and it can be seen that the controller was able to reset the offset after about 2.5 minutes. Once again the controller proved to be effective and efficient in maintaining the set point.

- Flow distribution for non-uniform heat load

To evaluate the effect of a non-uniform heat load applied to the MEs on the flow distribution and,

consequently, on the pseudo chips' temperature and performance of the controllers, tests were developed for different heat loads between 30 W and 90 W and set points of outlet vapor quality between 15% and 22%. A total of eight different combinations of heat loads and three outlet vapor qualities were evaluated, as can be seen in the Figure 22.

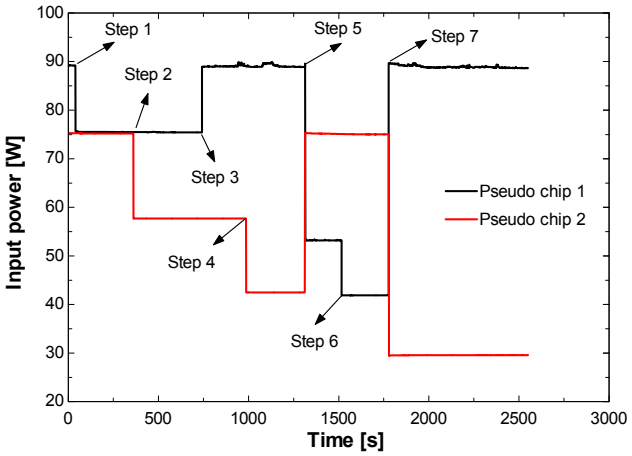

Figure 22 Different heat loads on the MEs

The tests started with the *standard conditions*, a set point of condensing pressure and outlet vapor quality of 16.8 bar and 22%, and a heat load on the ME1 and ME2 of 90 W and 75 W, respectively. Seven steps of heat load were then imposed, with the last one considering three different vapor quality set points; 22%, 18% and 15%. The steady state condition was obtained before each change in heat load or set point of vapor quality. Figures 23 and 24 show the results obtained for the average temperature on the pseudo chips, the MEs' outlet vapour qualities and the A_{SMV} (action of the controller).

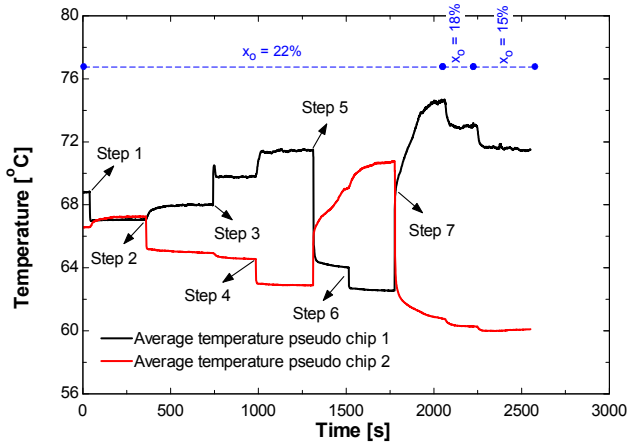

Figure 23 Average temperature on the pseudo chips

Firstly, it can be seen that the SMV controller was effective and efficient in controlling the outlet vapor quality under different conditions of heat load and set points of exit vapor quality. The controller proved to be very fast in reaching the steady state condition, with the maximum transient time observed to be about 30 s in step 7.

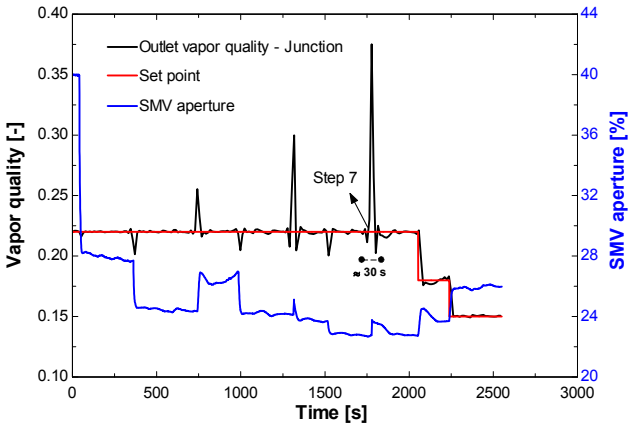

Figure 24 Outlet vapour quality and SMV aperture

Regarding the pseudo chips' temperatures (*viz.* Figure 23), the following was observed:

a) For the same heat load, step 2, the average temperature of both pseudo chips was the same, i.e. about 67 °C. This implies that the distributors (piping) before and after the MEs were well designed and that both MEs have the same mass flow rate.

b) The maximum temperature difference observed was, as expected, in step 7, which considered 90 W on chip 1 and 30 W on chip 2. A difference of 14.5 °C was obtained, where chip 1 reached a temperature of 75 °C vs 60.5 °C on chip 2. Despite this difference, the limit of 85 °C is still very far away.

c) The chips' temperature difference and the absolute temperatures were reduced when the set point of the outlet vapor quality was reduced. A difference of 11.5 °C and a temperature of 71.5 °C was obtained for chip 1 when the outlet vapor quality set point was reduced to 15%.

Figure 25 shows the effect of non-uniform heat load on the LPS controller. It can be seen that for all ranges of heat load investigated, the controller was able to control and stabilize the condensing pressure at the set

point. The maximum disturbance observed was stabilised after 5 min and provoked an overshoot of only 0.1 °C in the condensing temperature.

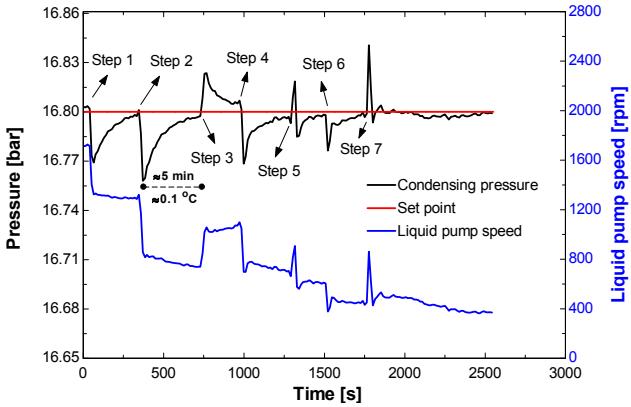

Figure 25 Condensing pressure and LPS

Finally, it can be highlighted that the dualSISO strategy proved to be a simple and effective way of controlling the condensing pressure and vapor quality while maintaining the chips within a safe operating range. The coupling effect between the two controllable variables was not strong, in other words the controllers have low interaction effects, implying that it was not necessary to apply a more complex centralized MIMO controller.

5.2. Vapor compression cooling system

For the vapor compression cooling system, alternative control strategies were adopted due to its cooling cycle concept being different. In this system the objective is not only to cool the pseudo chips but also to recover the energy removed in the condenser, since a higher condensing temperature is possible to be obtained (higher exergy available). From this point of view, the difference in temperature between outlet water flow and inlet working fluid flow in the condenser (ΔT_c) and the MEs' outlet vapor quality were defined as the variables to be controlled. The manipulated variables were, for the former, the LPS and for the latter the SMV aperture and the minicompressor stroke. It is worth mentioning that preliminary evaluations for the LPS controlling the condensing pressure were developed, as used in the liquid pumping cooling system. However, this variable showed a strong coupling with the outlet vapor quality, which provoked instabilities in the system when the controllers were operated together.

The SMV was used as an expansion device (EEV in Figure 4) and also as an actuator to control the outlet vapor quality together with the minicompressor. The results obtained in this work, as will be shown, proved that since the system is well designed and controlled, a SMV for each ME is not necessary, as was initially proposed by [16] and schematically given in Figure 4, i.e. only one SMV or EEV is sufficient to operate as an expansion device and actuator for the outlet vapor quality controller. The minicompressor is a linear oil free compressor capable of modulating the volumetric displacement, here defined as the stroke, which can be modulated, according to the manufacturer's scale, between zero and ten.

Regarding the thermodynamic conditions at the inlet of the minicompressor and MEs, all tests presented in this work showed superheating and subcooling conditions, respectively. The values remained between 1 °C and 10 °C, and in the same way as was observed in the previous system, special controllers were not required to avoid saturation conditions. The reason is partly associated with the performance obtained by the iHEx and LPR components (*viz.* Figure 4). As will be discussed, they showed a high exergetic efficiency and consequently ensured the conditions mentioned beforehand.

A. Controllers

- SMV and minicompressor controllers

System identification, controller design and reference tracking evaluation were done, as for the previous system. To control the MEs'outlet vapour quality, the SMV aperture and the minicompressor stroke were used as manipulating variables. Therefore, two PI controllers were designed independently. The SMV controller used the same strategy, i.e. a gain-scheduling PI controller whose parameters are actualised for each acquisition time. The relation between the manipulated and the controlled variables can be considered static, which is a function of the SMV and is given by Equation 9 (static gain K_p):

$$K_P = \frac{\partial X}{\partial SMV} = 3.5.10^{-2} SMV^3 - 1.1 SMV^2 + 10.9 SMV - 36.2 \quad (9)$$

The gains of the controller are a function of the gain K_p according to Equations 7 and 8. The desired closed loop time constant was adjusted to τ_D = 15 s, the

constant $C = 35$ and the *anti-wind up* set to 0.5. Due to the SMV operating as an expansion device, the range of operation was limited between 6.5% to 9% of aperture.

For the minicompressor controller, the transfer function obtained from the system identification is given by:

$$G(s)=\frac{y(s)}{u(s)}=\frac{-0.0573e^{-0.0741s}}{8.23s+1} \quad (10)$$

Using the linear programming method proposed in [31] and considering a phase margin of 60°, a gain margin of 2 and a crossover frequency twice as large as in the open loop, the minicompressor's PI parameters, i.e. K_C and T_I, were determined as -34.3%/stroke and 8.23 s, respectivelly.

- LPS controller

To control the difference of temperature between outlet water flow and inlet working fluid flow in the condenser, i.e. ΔT_c, the LPS was used as the manipulating variable. The transfer function obtained from the system identification is given by Equation 11, and the LPS controller parameters adjusted were 82.04 °C/rpm and 33.76 s, respectivelly for K_C and T_I. The same criteria and method used for the design of the minicompressor controller was used:

$$G(s)=\frac{y(s)}{u(s)}=\frac{0.0234e^{-0.01s}}{33.76s+1} \quad (11)$$

- Controllers evaluation

A *standard condition* was defined to start each evaluation, i.e., minicompressor stroke of 4, SMV aperture of 7.7%, LPS of 1100 rpm, inlet water temperature in the condenser of 14 °C and input powers of 75 W, 75 W and 150 W on pseudo chips 1 and 2, and on the post heater wrapped on the piping after the MEs (HS in the Figure 4), respectively.

The post heater was necessary to guarantee superheated conditions at the inlet of the VSC and subcooled liquid at the inlet of the MEs. The post heater simulates the auxiliary electronics described beforehand and in [16]. A fixed value of 125 W was used, which, combined with the input power on the pseudo chips, added up to a total heat load of about 290 W, which is equivalent to the heat load associated with IBM's QS22 blade.

Figures 26 and 27 show the results for the MEs' outlet vapor quality tracking test, where ΔT_c was set to the value of 15 °C. The *standard condition* was defined as the starting point and six steps of vapor quality between 40% to 60% were investigated.

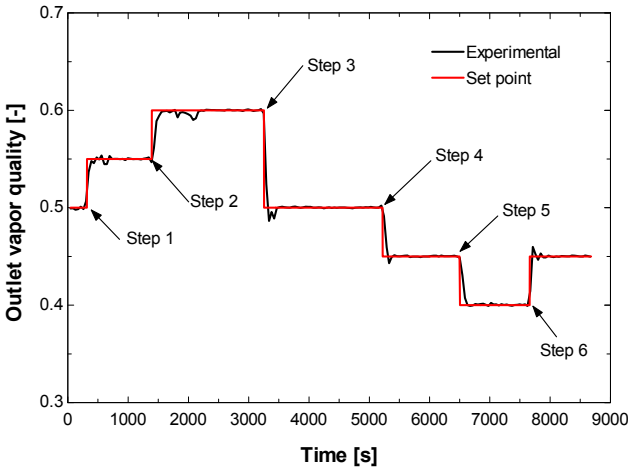

Figure 26 Outlet vapor quality tracking test

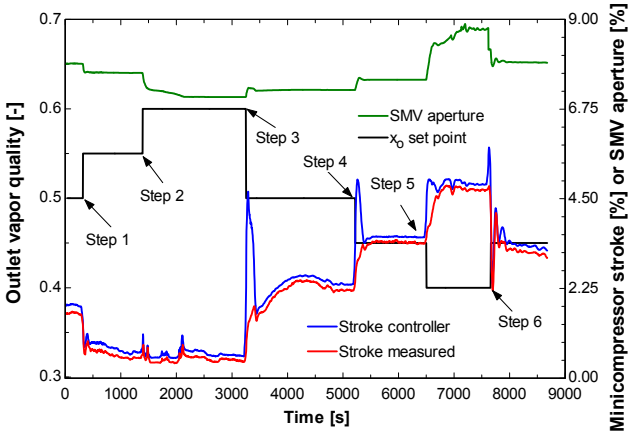

Figure 27 SMV and minicompressor actuators

The outlet vapor quality proved to be well controlled by the two actuators operating together. It can be said that a neglegible overshoot was observed and the controllers, minicompressor and SMV, are efficient and effective in tracking the outlet vapor quality since no instabilities were observed in the outlet vapor quality. In the worst case, i.e. step 3, the controller took about 60 s to stabilize the system.

An anomalous operation was observed in the controller of the minicompressor, as can be seen in

Figure 27. When the minicompressor controller tried to increase the stroke, defined by the stroke controller, the actual stroke or stroke measured did not respond as defined by the controller. Such a situation was observed during steps 3, 4 and 5, which certainly has some negative effect in the performance of the controller, which was not observed in the present work probably due to the SMV controller compensating this deficiency. The reason probably is that the minicompressor was not designed for so extreme operation point (evaporation of about 60 °C and condensation of about 80 °C).

Figure 28 shows the effect of x_o tracking tests on the LPS controller, where it can be observed that the coupling effect between the controlled variables ΔT_c and x_o was negligible, since the controller was shown to be effective and efficient in maintaining the desired ΔT_c set point. The maximum overshoot observed for such a controller was ±0.2 °C.

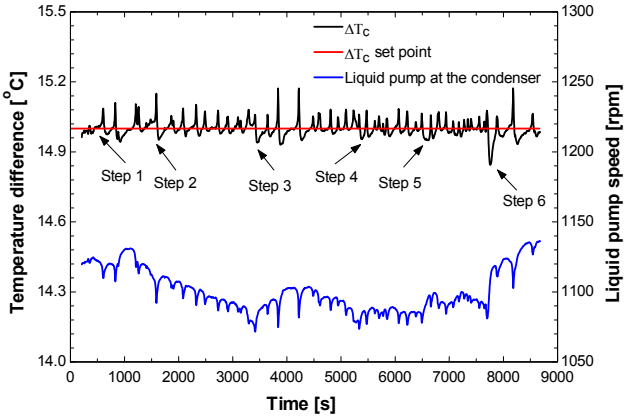

Figure 28 Evaluation of coupling effect between ΔT_c and x_o.

B. SISO-SIMO controller

The controllers designed previously, LPS controller (SISO strategy) and minicompressor and SMV controllers (SIMO strategy), were integrated and evaluated through heat load disturbance rejection and flow distribution tests. The *standard condition* previously defined was used as a starting point. Figure 29 shows the block diagram that represents such an integrated control strategy.

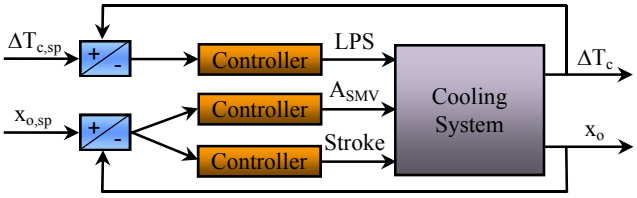

Figure 29 The SISO-SIMO controller.

- Heat load disturbance rejection

The heat load disturbance tests followed the same inputs considered for the previous system, i.e. periodic changing in the heat load on the MEs for a time period of 1.4 s. The input power changed between 75 W and 90 W on pseudo chip 1 and 75W and 60 W on pseudo chip 2. The set point of x_o was considered to be 45%. Figures 30 to 32 show the results obtained for the average temperature of the pseudo chips, the variables under control (ΔT_c and x_o) and the action of the controllers.

The maximum temperature variation observed was 1.5 °C, the same as for the previous system (*viz.* Figures 19 and 30). Additionally, as can be seen in Figure 31, the SIMO controller, i.e. the SMV and minicompressor actuators controlling x_o, was effective in controlling x_o, showing a continuous process of searching associated with the periodic changing in the heat load. The maximum variation of x_o regarding the set point was only 5%. It was also observed that the SMV controller did not show any adverse effect on this test, with its aperture remaining constant.

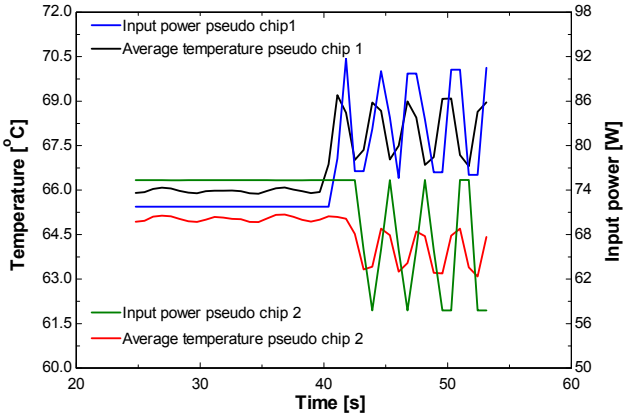

Figure 30 Heat load disturbance and pseudo chips temperature

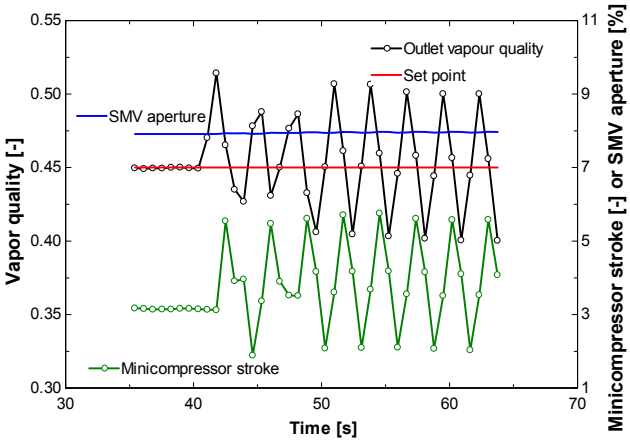

Figure 31 Outlet vapor quality and SMV and minicompressor's controllers

The coupling effect between the parameters being controlled once again proved to be negligible, as can be seen in Figure 32. To conclude, the integrated SISO-SIMO controller proved to be effective in the rejection disturbance of heat load, ensuring the stability of the system inside an acceptable level, i.e. the system control did not show instabilities or loss of control.

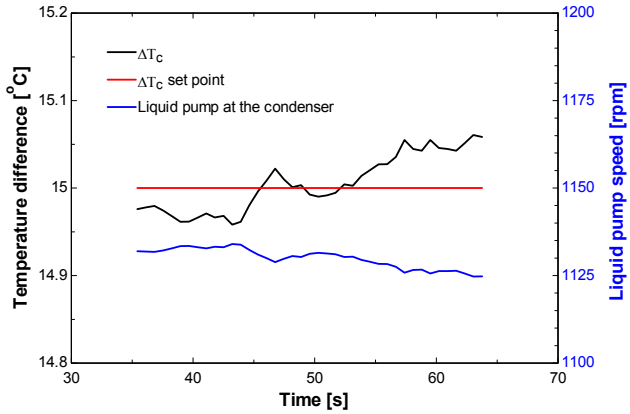

Figure 32 ΔT_c and LPS controller

- Flow distribution for non-uniform heat load

To evaluate the effect of unbalanced heat loads on the pseudo chips' temperature and the controlability of the vapor compression cooling system, four different steps were given in the input powers to pseudo chips 1 and 2, which were changed between 40 W and 90 W. The set point of x_o and ΔT_c were fixed at 45% and 15 °C, respectively. Figures 33 to 36 show the input power changes, the average temperature of the pseudo chips and the action of the controllers to maintain the controllable parameters at their respective set points.

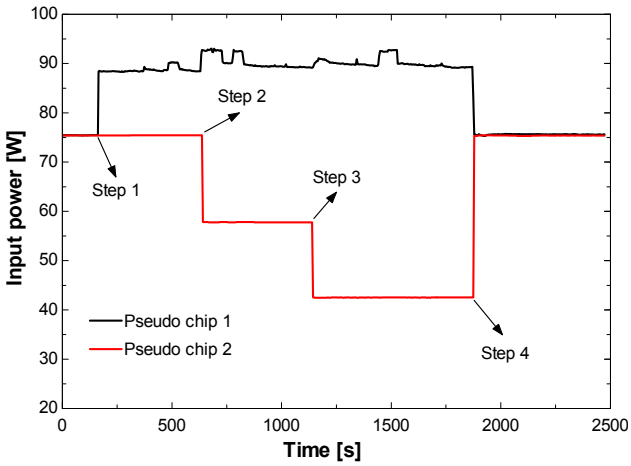

Figure 33 Different heat loads on the MEs

It can be observed from Figures 33 and 34 that the difference of temperature between the chips increases when the difference in the applied input power increases. A higher heat load on one of the MEs generates a higher outlet vapor quality. To maintain the same pressure drop between the two MEs, which are in parallel flow, the mass flow rate needs to be reduced, with the consequence that there is an increase in temperature due to a decrease in the heat transfer coefficient.

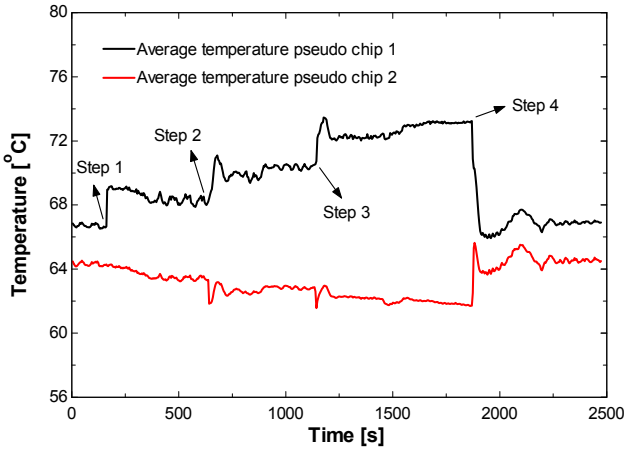

Figure 34 Average temperatures on the two pseudo chips

The highest difference observed was for step 3, where, after steady state has been reached, a difference of 12 °C was observed. However, the limit of 85 °C was still far away.

The SIMO controller, which uses the SMV and minicompressor as actuators, proved to be effective and efficient in controlling x_o. The maximum overshoot observed in step 4 was only 0.07% in vapor quality (*viz.* Figure 35). In this case, especially for steps 1 and 4, it can be seen that the SMV showed a more pronounced change in the aperture when compared with that obtained in the disturbance rejection tests. The SMV actuator can be seen as a fine adjustment of x_o. The anomalous operation to adjust/control the minicompressor's stroke continued, i.e. the actual stroke is shorter than that requested by the controller.

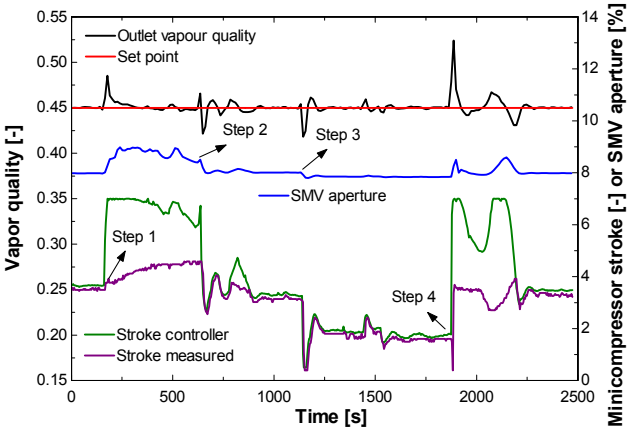

Figure 35 Outlet vapour quality and SMV aperture

Regarding the LPS controller, it can be seen from Figure 36 that it was effective in maintaining the 15 °C set point, independent of changes in the heat loads on the MEs. The maximum overshoot remained between ± 0.5 °C while no instabilities were observed.

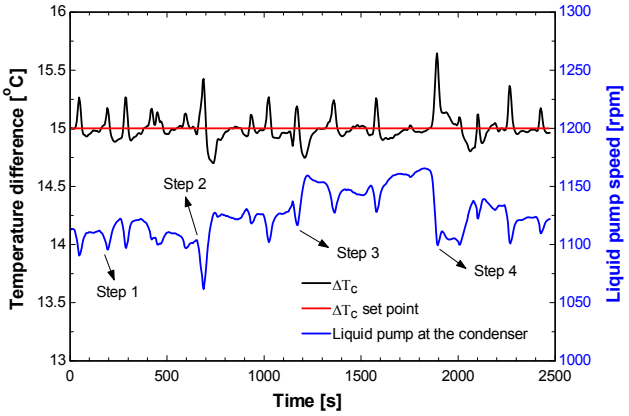

Figure 36 ΔT_c and LPS controller

Additionally and finally, the effect of the ΔT_c set point on the water temperature at the outlet of the condenser was investigated. The main interest in such an analysis is the exergy available in the condenser, which increases when the water temperature increases. Three set points were tested, i.e. 15 °C, 10 °C and 7.5 °C. The results can be seen in Figure 37. The heat load on the MEs was fixed at 75 W, the x_o set point at 50% and a steady state condition was considered for this analysis.

As can be seen, an increase of about 14°C was obtained in the outlet water temperature, which represents a much higher economic value for the energy recovered in the condenser. It also demonstrates the versatility of such a system in changing the set points without compromising the cooling cycle performance and pseudo chip temperatures, which hardly varied when the ΔT_c set point was changed. The following section shows a comparative analysis between the two cooling systems evaluated, where a deeper investigation of exergy is made.

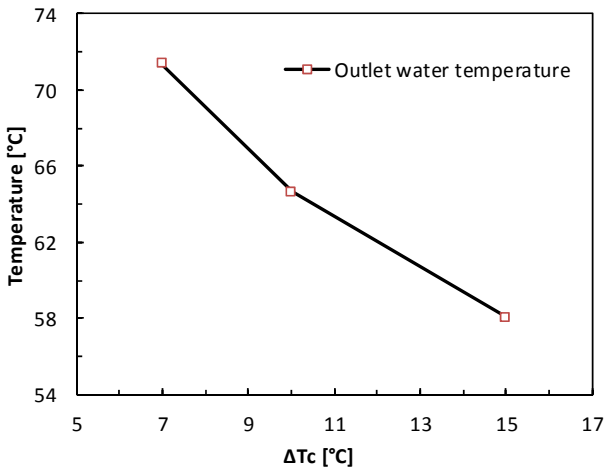

Figure 37 Outlet water temperature vs ΔT_c set point

5.3. Comparative analysis

To compare the performance of the liquid pumped and vapor compression cooling systems, which were experimentally evaluated and analysed beforehand, a steady state condition was selected from the flow distribution tests. Such a comparison mainly evaluates the difference between the power consumption of the drivers and the available energy and exergy in the condenser. The experimental condition selected for the comparison was that the input powers on pseudo chips 1 and 2 were 90 W (41.7 W/cm^2) and 75 W

(34.7 W/cm^2), respectively.

A. Power consumption

Table 1 shows the results for the driver's power consumption and overall efficiency, the latter calculated as the ratio between the isentropic pumping or compression and the eletrical input power. It also shows the two systems' input and output energies associated with components and piping and the thermodynamic conditions in the condenser for the main and secondary working fluids.

Table 1 Energy in and out in the systems and thermodynamic conditions in the condenser.

Energy in	LP cycle	VC cycle
Pump or compressor input power, W	17.42	102.12
Isentropic pumping or compression power, W	0.048	27.77
Driver overall efficiency, %	0.28	27.19
Inverter power consumption, W	10.0	-
Electrical efficiency, %	42.58	-
Mechanical power consumption, W	7.42	-
Mechanical efficiency, %	0.65	-
Input power on the pseudo chips, W	164.47	164.51
Input power on the post heater, W	0	125.63
SMV input power, W	0.49	0.95
Energy out	**LP cycle**	**VC cycle**
Heat transfer in the condenser, W	68.32	194.23
Heat loss in the driver, W	17.37	74.35
Heat loss in the piping, W	96.68	124.63
Thermodynamic conditions in the condenser		
Condensing temperature, °C	59.96	80.48
Inlet water temperature, °C	39.96	14.61
Outlet water temperature, °C	49.32	65.04
Mass flow rate of water, kg/h	6.28	3.31

The results showed a higher driver's input power for the VC system, about 6 times higher, which naturally is associated with the energy expended to maintain the difference of pressure between the condenser and micro-evaporator. It is worth observing the drivers' low overall efficiency, which for the pump is mainly a consequence of leakage and slip of HFC134a in the gears. Such a characterisitc is due to the low viscosity of the working fluid, being at the lower limit for the specified pump (hence a better pump would be advisable). As can be seen in Table 1, the mechanical efficiency is also very low, which confirms such an observation.

Regarding the minicompressor, despite the high overall efficiency, it is actually considered to be low, especially when compared with conventional household compressors, which have values normally between 50% and 70%. Such a low efficiency is potentially associated with the fact that the minicompressor is operating at much higher suction/discharge pressures than its actual design conditions.

It can also be seen that about 50% and62 % of the energy out of the VC and LP systems, respectively, are associated with heat losses. It shows that improvements can be done to improve the overall performance of the system, which would mainly be associated with the reduction of the driver and piping losses and, consequently, to increase the energy recovered in the condenser.

Finally the results showed a much higher temperature for the secondary fluid at the outlet of the condenser when using the VC system, which is related to the higher condensing temperature. This implies that a higher economic value is obtained for the energy available in the condenser. The analyses that follows will show the advantage of such a system when evaluating it from an exergy's point of view.

B. Energy recovery

To better explore and understand the difference between the two possibilities of cooling systems (vapor compression and liquid pumping) regarding energy recovery, i.e. exergy available in the condenser for a secondary application, the concept of exergy is introduced.

The steady state exergy rate balance is defined by Equation 12 [34]. The first and second terms in the right side of the equality represent the exergy transfer accompanying heat and work, the third and fourth are the time rate of exergy transfer accompanying mass flow and flow work and, finally, the last term is the

rate of exergy destroyed:

$$0 = \underbrace{\sum_j \left(1 - \frac{T_0}{T_j}\right) \dot{Q}_j - \dot{W}_{cv} + \sum_i \dot{m}_i e_{fi} - \sum_e \dot{m}_e e_{fe}}_{rate\ of\ exergy\ transfer} - \underbrace{\dot{E}_d}_{\substack{rate\ of \\ exergy \\ destruction}} \quad (12)$$

where:

T_0 - dead state temperature
T_j - instantaneous temperature
$\dot{Q}_j$ - heat transfer rate
$\dot{W}_{cv}$ - energy transfer rate by work
$\dot{m}_i$,$\dot{m}_e$ - inlet and outlet mass flow rate
$\dot{e}_{fi}$, $\dot{e}_{fe}$ - inlet and outlet flow exergies
$\dot{E}_d$ - rate of exergy destruction due to irreversibilities within the control volume

It can be observed that an exergy reference environment is necessary to be defined. Such an environment represents the state of equilibrium or dead state. This equilibrium state defines the exergy as the maximum theoretical work obtainable when another system in a non-equilibrium state interacts with the environment to the equilibrium. For the present work the reference is defined as 295 K, 100 kPa for water and 295 K, 603.28 kPa and 50% of vapor quality for HFC134a.

The goal of the analysis is to determine, for each system, the exergy supplied, recovered and destroyed for a control volume enclosing the cooling system. With this, the overall exergetic efficiency, defined as the ratio between the recovered and supplied exergies, can be determined. The exergetic efficiency of each component is also evaluated. It qualitatively identifies and classifies the components that present higher irreversibilities, helping to decide which component to optimize to improve the thermodynamic performance of the cooling cycle. Table 1 from the previous section and Table 2 show the results obtained regarding energy and exergy, respectively.

Table 2 Exergetic analysis for the VC and LP cooling systems.

	LP cycle	VC cycle
Exergy supplied, W	40.1	146.7
Exergy destroyed or irreversibility, W		
Pump or compressor	17.4	74.4
Condenser	3.5	21.4
ME1	3.4	3.6
ME2	0.9	0.8
Post heater	----	9.0
iHEx	----	1.3
LPR	----	0.9
SMV	0.27	3.3
Piping	9.7	21.3
Total	35.2	136.0
Exergy recovered, W	**4.9**	**10.7**
Exergetic efficiency, %		
Pump or compressor	0.03	27.2
Condenser	58.4	33.6
ME1	72.6	70.7
ME2	90.7	91.1
Post heater	----	59.3
iHEx	----	78.8
LPR	----	72.7
SMV	----	----
Piping	----	----
Overall	**12.3**	**7.3**

Firstly, it can be seen that the total exergy recovered is higher for the VC cooling system, which is a consequence of the higher exergy supplied by the driver and the exergy of the post heater, where the latter was not being considered in the LP system's experimental tests. However, it is highlighted that this high exergy is the subject of interest of the owner of a secondary application of the recovered heat.

Regarding the exergetic efficiency of the components considered in the cooling systems, the driver followed by the condenser showed the lowest values, which implies that to improve the thermodynamic performance of the cooling systems such a components must be optimized in the design. Special attention must also be given to the exergy destroyed in the piping, which represents about 28% and 16% of the overall exergy destroyed in the LP and VC systems, the latter being the same order of magnitude

as that in the condenser. This implies that a better insulation of the test unit is required to minimize the heat losses, i.e. exergy lost or destroyed.

It can also be observed that the overall exergetic efficiency was lower for the VC cooling system, with the compressor, condenser and piping being the main culprits. The overall exergetic efficiency also shows that there is a huge need to improve the thermodynamic performance of the cooling systems, since only an average of 10% of the supplied exergy is used.

The results and analyses shown previously may lead one to conclude that the LP system is better in terms of exergy and energy. However, such a conclusion is not fair, especially when looking for the potential to improve the components' exergetic efficiency and to reduce the piping's exergy destroyed. It seems both systems can be optimized, i.e. better designed so that improvements will be generated, since the present setups were the first of a kind. It is also important to mention that the results shown here represent only the initial step in a much larger experiment campaign and this more extensive experimental campaign will be used to generalize the results.

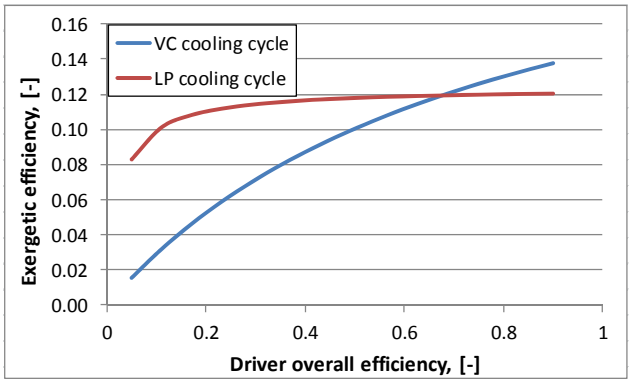

Figure 38 Exergetic efficiency versus driver overall efficiency

To consider the effect of an improvement in the drivers' overall efficiency (the worst component in terms of exergetic efficiency) on the overall exergetic efficiency of the systems, a thermodynamic simulation was developed considering as inputs the experimental results used in the previous analysis. Figure 38 shows the results, where can be seen that the effect on the exergetic efficiency is much higher when using a VC as a driver and that there is a point where the exergetic efficiency of the VC system surpasses that of the LP system (at about 65%). From an exergetic point of view, only after this point the VC cooling system is competitive with the LP cooling system. It is also important to remember that the other exergy losses must be considered and the matching point of exergetic efficiency showed in Figure 38 can be changed to higher or lower values in that case.

Finally, it is important mentioning that the thermodynamic performance alone (energy balance) does not permit implementing the analysis shown beforehand. Exergy analysis clearly identifies efficiency improvements and reductions in thermodynamic losses attributable to green technologies. Additional advantages of such analyses are the potential to evaluate green technology aspects such as environmental impact or sustainable development (normally associated with carbon dioxide emissions) and economics ("exergy, not energy, is the commodity of value in a system, and assign costs and/or prices to exergy-related variables."[35]).

6. Conclusion

Two specific on-chip two-phase cooling cycles described by [16] were built in the LTCM lab and experimentally tested and evaluated. The main difference of the two systems tested regards the driver. A liquid gear pump and a minicompressor were assembled in the system and aspects such as energy consumption, exergetic efficiency and controllability were investigated. The first step was to design specific controllers for the ME's outlet vapor quality, condensing/evaporating pressure and difference of temperature between outlet water flow and inlet working fluid flow in the condenser (ΔT_c). The controllers designed were evaluated by tracking and disturbance rejection tests, which were shown to be efficient and effective. The average temperatures of the pseudo chips were maintained below the limit of 85 °C for all tests evaluated in steady state and transient conditions. Additional tests were also done considering a periodic change of heat load, where the maximum variation observed in the average temperature of the pseudo chips was only 1.5 °C.

In general, simple SISO strategies were sufficient to attain the requirements of control, i.e. more complex MIMO strategies were not necessary for this

application. Regarding energy and exergy analyses, the experimental results showed that both systems can be thermodynamically improved since only about 10% of the exergy supplied is in fact recovered in the condenser in the present setup. Additional analysis highlighted the effect of the ΔT_c set point on the water temperature (secondary fluid) at the outlet of condenser. The results showed that temperatures higher than 70 °C can be obtained when the ΔT_c set point is reduced from 15 °C to 7 °C without compromising the cooling system performance and pseudo chip temperatures, which is interesting when the subject of energy recovery is considered. It also shows the mandatory character of the minicompressor, i.e. to be able to operate the system with higher condensing temperatures (exergy available). Finally, the results presented were not generalised since only a limited number of tests were done and a more detailed experimental campaign is necessary to better describe and compare both systems presented.

6. Acknowledgements

The Swiss Commission for Technology and Innovation (CTI) contract number 6862.2 DCS-NM entitled "Micro-Evaporation Cooling System for High Performance Micro-Processors: Development of Prototype Units and Performance Testing" directed by the LTCM laboratory sponsored this work along with the project's industrial partners: IBM Zürich Research Laboratory (Switzerland) and Embraco (Brazil). J.B. Marcinichen wishes to thank CAPES ("Coordenação de Aperfeiçoamento de Pessoal de Nível Superior") for a one year fellowship to work at the LTCM laboratory. The authors also wish to thank the engineer Vinícius de Oliveira from the Automatic Control Laboratory (EPFL - Lausanne - Switzerland) for support in the development of the control tools.

References

[1] Olivier, J.A., Marcinichen, J.B and Thome, J.R., 2010, "Two-phase Cooling of Datacenters: Reduction in Energy Costs and Improved Efficiencies", in Proceedings of the 13th Brazilian Congress of Thermal Sciences and Engineering – ENCIT2010, Uberlandia, MG, Brazil.

[2] Agostini, B., Fabbri, M., Park, J.E., Wojtan, L., Thome, J.R. and Michel, B., 2007, "State of the Art of High Heat Flux Cooling Technologies", Heat Transfer Engineering, Vol. 28, pp. 258-281.

[3] EPA, Report to Congress on Server and Data Center Energy Efficiency Public Law 109-431. 2007, U.S. Environmental Protection Agency.

[4] Larson, J.B., America's Energy Security Trust Fund Act of 2009. 2009: H.R. 1337.

[5] Koomey, J.G., Estimating Total Power Consumption by Servers in the U.S. and the World. Analytics Press, 2007. Oakland, CA, February 15. (http://enterprise.amd.com/us-en/AMD-Business/Technology-Home/Power-Management.aspx).

[6] Hannemann, R., Marsala, J. and Pitasi, M., 2004, "Pumped Liquid Multiphase Cooling", in Proceedings IMECE - International Mechanical Engineering Congress and Exposition, Anaheim, CA, USA, paper 60669.

[7] Mongia, R., Masahiro, K., DiStefano, E., Barry, J., Chen, W., Izenson, M., Possamai, F., Zimmermann, A. and Mochizuki, M., 2006, "Small Scale Refrigeration System for Electronics Cooling within a Notebook Computer", in Proceedings ITHERM, San Diego, CA.

[8] Trutassanawin, S., Groll, E. A., Garimella, S.V. and Cremaschi, L., 2006, "Experimental Investigation of a Miniature-Scale Refrigeration System for Electronics Cooling", IEEE Transactions on Components and Packaging Technologies, Vol. 29, N°3, pp. 678-687.

[9] Thome, J.R., Agostini, B., Revellin, R. and Park, J.E., 2007, "Recent Advances in Thermal Modeling of Micro-Evaporators for Cooling of Microprocessors", in Proceedings of the ASME International Mechanical Engineering Congress and Exposition (IMECE), Seattle, Washington.

[10] Agostini, B., Fabbri, M., Thome, J.R., Michel B., 2008, "High Heat Flux Two-Phase Cooling in Silicon Multimicrochannels", IEEE Transactions on Components and Packaging Technologies, Vol. 31, N° 3, pp. 691-701.

[11] Thome, J.R. and Bruch, A., 2008, "Refrigerated Cooling of Microprocessors with Micro-Evaporation Heat Sinks: New Development and Energy Conservation Prospects for Green Datacenters", in Proceedings Institute of Refrigeration (IOR).

[12] Mauro, A.W., Thome, J.R., Toto, D. and Vanoli, G.P., 2010, "Saturated Critical Heat Flux in a Multi-Microchannel Heat Sink Fed by a Split Flow System", Experimental Thermal and Fluid Science, Vol.34, pp. 81-92.

[13] Park, J.E. and Thome, J.R., 2010, "Critical Heat Flux in Multi-Microchannel Copper Elements with Low Pressure Refrigerants", Int. J. Heat Mass Transfer, Vol.53, pp. 110-122.

[14] Zhou, R., Zhang, T., Catano, J., Wen, J.T., Michna, G.J., Peles, Y. and Jensen, M.K., 2010, "The Steady-State Modeling and Optimization of a Refrigeration System for High Heat Flux Removal", Applied Thermal Engineering, doi: 10.1016/j.applthermaleng.2010.05.023.

[15] Zhang, T., Wen, J. T., Peles, Y., Catano, J., Zhou, R. and Jensen, M.K., 2011, "Two-Phase Refrigerant Flow Instability Analysis and Active Control in Transient Electronics Cooling Systems", International Journal of Multiphase Flow, Vol. 37, pp. 84-97.

[16] Marcinichen, J.B., Thome, J.R. and Michel, B., 2010. "Cooling of Microprocessors with Micro-Evaporation: A Novel Two-Phase Cooling Cycle", International Journal of Refrigeration.

[17] Marcinichen, J.B and Thome, J.R., 2010, "Refrigerated Cooling of Microprocessors with Micro-Evaporation New Novel Two-Phase Cooling Cycles: A Green Steady-State Simulation Code", in Proceedings of the 13th Brazilian Congress of Thermal Sciences and Engineering – ENCIT2010, Uberlandia, MG, Brazil.

[18] Ganapati, P., 2009. "Water-Cooled Supercomputer Doubles as Dorm Space Heater", Available from: http://www.wired.com/gadgetlab/2009/06/ibm-supercomputer/.

[19] Meijer, G.I., Brunschwiler, T., and Michel, B., 2009, "Using Waste Heat from Datacenters to Minimize Carbon Dioxide Emissions", ERCIM News, Vol. 79, pp. 23-24.

[20] Brunschwiler, T., Meijer, G.I., Paredes, S., Escher, W. and Michel, B., 2010, "Direct Wast Heat Utilization from Liquid-Cooled Supercomputers", Proc. 14th Int. Heat Transfer Conference, Aug. 8-13, Washington, DC, USA.

[21] Morini, G.L., 2006, "Scaling Effects for Liquid Flows in Microchannels", Heat Transfer Engineering. Vol. 27: pp. 64-73.

[22] Revellin, R., Dupont, V., Ursenbacher, T., Thome, J.R., and Zun, I., 2006, "Characterization of Two-Phase Flows in Microchannels: Optical Measurement Technique and Flow Parameter Results for R-134a in a 0.5 mm Channel", International Journal of Multiphase Flow, Vol. 32: pp. 755-774.

[23] Ong, C.L. and Thome, J.R., , 2011 "Macro-to-Microchannel Transition in Two-Phase Flow: Part 1 - Two-Phase Flow Patterns and Film Thickness Measurements", Experimental Thermal and Fluid Science, Vol. 35: pp. 37-47.

[24] Madhour, Y., Olivier, J.A., Costa-Patry, E., Paredes, S., Michel, B., and Thome, J.R., Flow Boiling of R134a in a Multi-Microchannel Heat Sink with Hotspot Heaters for Energy-Efficient Microelectronic CPU Cooling Applications. IEEE Transactions on Components and Packaging Technologies, Accepted for publication, 2010.

[25] Agostini, B., Revellin, B. and J.R. Thome, 2008, "Elongated Bubbles in Microchannels. Part I: Experimental Study and Modeling of Elongated Bubble Velocity", Int. J. Multiphase Flow, Vol. 34, pp. 590-601.

[26] Borhani, N., Agostini, B. and Thome, J.R., 2010, "A Novel Time Strip Flow Visualization Technique for Investigation of Intermittent Dewetting and Dryout in Elongated Bubble Flow in a Microchannel Evaporator", Int. J. Heat Mass Transfer, Vol. 53, pp. 4809-4818.

[27] Costa-Patry, E., Olivier, J., Michel, B. and Thome, J.R., 2011, "Two-Phase Flow of Refrigerants in 85µm-wide Multi-Microchannels: Part II – Heat Transfer with 35 Local Heaters", Int. J. Heat and Fluid Flow, Vol. 32, pp. 464-476.

[28] Revellin, R. and Thome, J.R., 2008, "A Theoretical Model for the Prediction of the Critical Heat Flux in Heated Microchannels", Int. J. Heat Mass Transfer, Vol. 51, pp. 1216-1225.

[29] Wolverine. Wolverine Tube Inc. 2010; Available from: www.wlv.com.

[30] IBM BladeCenter QS22: Overview. Available from: www-03.ibm.com/systems/bladecenter/hardware/servers/qs22/.

[31] Karimi, A., Kunze, M. and Longchamp, R., 2007, "Robust Controller Design by Linear Programming with Application to a Double-Axis Positioning System", Control Engineering Practice, Vol. 15, N° 2, pp. 197-208.

[32] Olivier, J.A., Thome, J.R., 2010, "Two-Phase Cooling of Electronics with Multi-Microchannel Evaporators", NATO: AVT - 178 Specialists' Meeting on System Level Thermal Management for Enhanced Platform Efficiency, Bucarest, Romania.

[33] Kunze, M., Karimi, A. and Longchamp, R., 2007, "Gain-Scheduled Controller Design by Linear

Programming", in Proceedings of the European Control Conference, Kos, Greece.

[34] Moran, M.J., Howard, I. and Shapiro, N., 2010, "Fundamentals of Engineering Thermodynamics", 6th ed., John Wiley & Sons, 725 pages.

[35] Rosen, M.A., Dincer, I. and Kanoglu, M., 2008, "Role of Exergy in Increasing Efficiency and Sustainability and Reducing Environmental Impact". Energy Policy, Vol 36: pp. 128-137.